

Impact of nanodroplets on cone-textured surfaces

Hanyi Liu (刘涵毅) ¹, Jun Zhang (张俊) ^{1,*}, Jia Luo (罗佳)¹, and Dongsheng Wen (文东升)^{1,2}

¹*School of Aeronautic Science and Engineering, Beihang University, Beijing 100191, China*

²*TUM School of Engineering and Design, Technical University of Munich, 80333 Munich, Germany*



(Received 24 December 2022; revised 13 March 2023; accepted 10 May 2023; published 6 June 2023)

Molecular dynamics simulations have been performed to study the dynamics of nanodroplets impacting on a flat superhydrophobic surface and surfaces covered with nanocone structures. We present a panorama of nanodroplet behaviors for a wide range of impact velocities and different cone geometries, and develop a model to predict whether a nanodroplet impacting onto cone-textured surfaces will touch the underlying substrate during impact. The advantages and disadvantages of applying nanocone structures to the solid surface are revealed by the investigations into restitution coefficient and contact time. The effects of nanocone structures on droplet bouncing dynamics are probed using momentum analysis rather than conventional energy analysis. We further demonstrate that a single Weber number is inadequate for unifying the dynamics of macroscale and nanoscale droplets on cone-textured surfaces, and propose a combined dimensionless number to address it. The extensive findings of this study carry noteworthy implications for engineering applications, such as nanoprinting and nanomedicine on functional patterned surfaces, providing fundamental support for these technologies.

DOI: [10.1103/PhysRevE.107.065101](https://doi.org/10.1103/PhysRevE.107.065101)

I. INTRODUCTION

Interest in, and demand for nanodroplet research has undergone a decade of rapid growth owing to the remarkable achievements in related applications at the nanoscale, such as electrochemical three-dimensional nanoprinting [1], spray cooling using nanoencapsulated phase-change materials [2], and even new concepts of cancer treatment by conjugating anticancer antibodies with the nanodroplets [3], to name a few. The necessity of obtaining a detailed understanding of nanodroplet dynamics is also driven by the fact that many models based on classical fluid dynamics fail at the nanoscale because of various scale effects [4–9]. Owing to the rapid development of computational facilities, molecular dynamics (MD) simulation is becoming one of the most widely used methods to probe complex dynamics of nanoscale flows (by solving the Newtonian equations of motion to track the trajectories of individual atoms). We strive for a better understanding of nanodroplet dynamics and complementary state-of-the-art nanoscale applications with the help of this powerful tool.

Nanodroplets impacting on solid surfaces is common in applications such as nanoprinting and nanomedicine, where droplets are used as the solvent for colloidal ink [10] or as a carrier of biological elements [11]. In these scenarios, nanodroplets require access to patterned surfaces of varying topological construct [12], and thus it is meaningful to probe the dynamics of nanodroplets on surfaces with different morphologies. Recent works relevant to nanodroplet impact focus mainly on flat surfaces with wettability gradients [13–16], on groups of flat surfaces with different wettabilities [12,17–25], or on textured surfaces covered with nanopillar

arrays [13,19,26–31]. Other interesting works involve inclined surfaces [32], moving surfaces [33], vibrating surfaces [34], stripe-textured surfaces [35], ridge-textured surfaces [36], point-textured surfaces [37], and spherical structures [38]. However, to the best of our knowledge, nanodroplet impact on the cone, which is another basic geometrical shape, has not yet been well studied. Since cone structures are ubiquitous in nature (e.g., pine needles) as well as in industry (e.g., the aeroengine rotating cone [39] and advanced bionic surfaces [40]), it is imperative to study the dynamics of nanodroplets impacting on such structures.

In addition to a relatively poor understanding of nanodroplets on cone-textured surfaces, there are two issues relevant to nanodroplet impact that are worth exploring. The first is the quantitative representation for nanodroplet rebound. Existing theoretical studies of nanodroplet impact dynamics have primarily utilized an energy-conservation-based approach. This approach employs a balance equation, namely,

$$E_k + E_{lv} + E_{sv} = E'_k + E'_{lv} + E'_{sl} + E_v, \quad (1)$$

that considers, on the left-hand side, the kinetic energy and interfacial energies (liquid-vapor and solid-vapor) at the initial state, and on the right-hand side, the kinetic energy, interfacial energies (liquid-vapor and solid-liquid) at any time instant after the droplet comes into contact with the solid surface, and viscous dissipation that occurs during this period. More elaborate models have been developed by better quantifying the solid-liquid interfacial energy (E'_{sl}) and the dissipation (E_v) terms. This has been achieved through various means, such as optimizing the flow-field distribution hypothesis when deriving E_v [41,42], or incorporating the effects of surface wettability into either the E'_{sl} [12,26,29] or E_v terms [20]. Obviously, accurately validating these

*Corresponding author: jun.zhang@buaa.edu.cn

energy-conservation-based models requires precise measurements of interfacial energy and viscous dissipation, which can be challenging to obtain through MD simulations. An alternative approach is to reframe these models in terms of the maximum spreading factor [12,20,26,29,41–43], which is defined as the ratio of the maximum spreading radius (which can be easily measured using MD) to the initial radius of a droplet, i.e., $\beta_{\max} = r_{\max}/R$. However, validating and applying these models in the case of rebound scenarios may still be challenging, as there is no morphological parameter akin to β_{\max} that fully characterizes the entire impact-rebound process of the droplet. The forces that a solid surface exerts on a nanodroplet, instead, are much more accessible than the interfacial and dissipation energy in MD simulations. Therefore, investigating the rebound dynamics of nanodroplets through the lens of momentum analysis holds promise and is a valuable pursuit.

Describing and comparing droplet behaviors across different scales is another intriguing challenge that needs to be effectively addressed. While the Weber number is the most commonly utilized dimensionless parameter for characterizing the impact dynamics of droplets at both macro- and nanoscales, little attention has been given to the differences in the impact dynamics of droplets with the same Weber number but varying sizes. Li and Zhang conducted both nanoscale MD simulations and macroscale experiments to investigate droplets impacting on superhydrophobic surfaces, and concluded that the trends of characteristic quantities (specifically, the β_{\max} , τ_c , and β_v vs the Weber number) were consistent between the simulation and experimental results [27]. Here and hereinafter, τ_c is the contact time between the droplet and solid surface, while $\beta_v = v_b/v_i$ is the restitution coefficient defined by the ratio of bounce velocity to impact velocity. However, other studies have shown that using a single Weber number is not sufficient for quantitative comparison of droplet dynamics across different scales—for instance, the critical Weber number required for nanodroplets to rebound [19,22,36] is significantly higher than for millimeter-sized droplets [44]. The limitations of utilizing a single Weber number for evaluating droplet dynamics can be attributed to the several distinct features [25] in nanodroplet impacts, with the amplified effects of viscous dissipation being the most notable—unlike millimeter-sized droplets that exhibit velocity gradients mainly in the boundary layer, nanodroplets display velocity gradients throughout their entire volume [41]. However, recent research has shown that the bulk viscous dissipation, previously considered a unique mechanism for nanodroplets, can also become dominant at the macroscale by increasing the liquid viscosity [45]. This suggests a simple but plausible approach to link the nanodroplet and macrodroplet dynamics, namely, by combining appropriate dimensionless parameters that accurately capture the contribution of various forces during droplet impact, without relying on the exploration of additional scale effects for the viscous dissipation.

In this work, we perform MD simulations to study the impact dynamics of nanodroplets on solid surfaces decorated with cone structures. We explore the behavior of nanodroplets over a wide range of impact velocities and cone geometries, and develop a model to predict whether a nanodroplet will touch the underlying substrate during impact. We evaluate

TABLE I. Parameters of the TIP4P/2005 model [49], where ξ_0 and σ_O are the Lennard-Jones parameters of oxygen; q_H and q_M are the charges of the hydrogen atom and the virtual massless site, respectively, and ε_0 is the vacuum permittivity.

ξ_0 (eV)	σ_O (Å)	q_H (e)	q_M (e)	ε_0 (F/m)
8.031×10^{-3}	3.159	0.5564	-1.1128	8.854×10^{-12}

the advantages and disadvantages of introducing nanocone structures to a solid surface by analyzing the restitution coefficient and contact time of the nanodroplets. Furthermore, we explore why nanocone structures can enhance the droplet bouncing, and propose a model based on momentum analysis that predicts whether a nanodroplet will rebound from a solid surface. Finally, we discuss a feasible approach to connect the dynamics of macrodroplet and nanodroplet, drawing on the recent research into millimeter-sized droplets impacting on cone structures [46] as a point of reference.

II. SIMULATION METHODS

All the MD simulations in this work are performed using the large-scale atomic/molecular massively parallel simulator (LAMMPS) [47], and the results are visualized using the open visualization tool (OVITO) [48]. The nanodroplets studied in this work are 32 Å in radius (R) and are composed of 4582 water molecules. Each water molecule is constructed with the acknowledged TIP4P/2005 model [49], for which the interactions between any two water molecules i and j are represented by a van der Waals term plus a Coulomb term, namely,

$$U_{ij} = 4\xi_0 \left[\left(\frac{\sigma_o}{r_{ij}} \right)^{12} - \left(\frac{\sigma_o}{r_{ij}} \right)^6 \right] + \frac{1}{4\pi\varepsilon_0} \sum_{a,b} \frac{q_a q_b}{r_{ab}}, \quad (2)$$

where r_{ij} is the distance between the Lennard-Jones centers (i.e., the oxygen atom), while a and b stand for the charged sites (including two hydrogen atoms and a virtual massless site) of two molecules. Other parameters in Eq. (2) are listed in Table I. The SHAKE algorithm [50] is applied to fix the oxygen-hydrogen bond length and the H-O-H bond angle as 0.9572 Å and 104.52°, respectively.

The solid surfaces are composed of copperlike atoms, which are fcc structured with a lattice constant $L_c = 3.615$ Å. The Lennard-Jones potential is implemented for the interaction between two solid atoms, with the parameters $\xi_{Cu} = 0.4093$ eV and $\sigma_{Cu} = 2.338$ Å [51], as well as for the interaction between the solid atoms and oxygen atoms, with the parameters determined by the Lorentz-Berthelot mixing rule, i.e., $\sigma_{Cu,O} = (\sigma_{Cu} + \sigma_O)/2$ and $\xi_{Cu,O} = k_\xi \sqrt{\xi_{Cu}\xi_O}$. In this work, we tune the scaling parameter k_ξ to simulate a superhydrophobic surface with an equilibrium contact angle $\theta_e = 158^\circ \pm 2^\circ$, which is identical to our macroscopic counterpart [46]. We refer the reader to Zhang *et al.* [52] for a detailed approach to measure the contact angles.

The initial system of the simulation is shown schematically in Fig. 1(a). Nanocones with a series of height and apex angle combinations are placed on the top of the flat substrate, where the height (H_{co}) ranges from 4 to 192 Å, and the apex angle (α) is set as 50°, 90°, 130°, and 170°. The distance

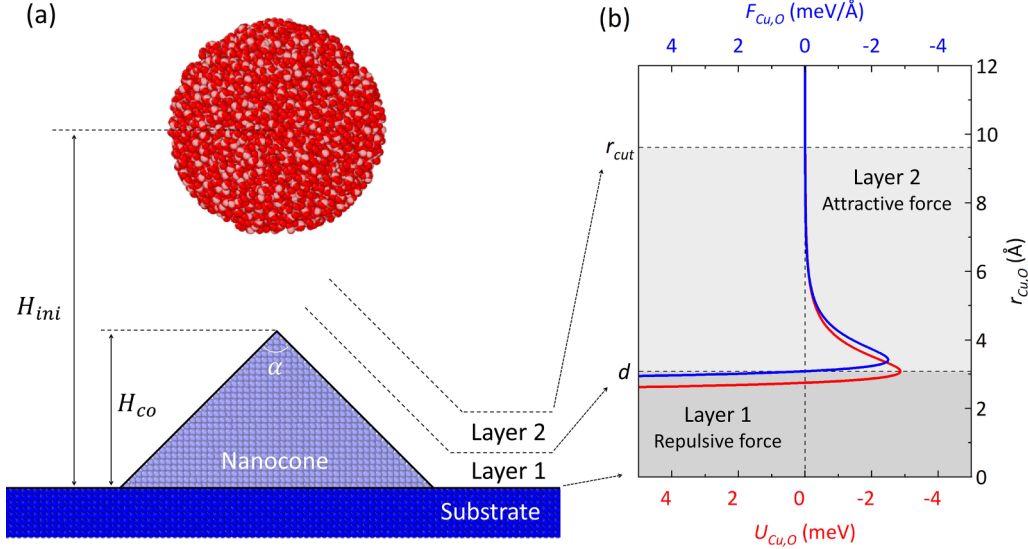


FIG. 1. (a) Schematic diagram of the initial system. The pink, red, and blue particles represent oxygen, hydrogen, and solid atoms, respectively. Note that the substrate (dark blue) and nanocone (light blue) consist of the same type of copperlike atoms, while the different coloring is provided solely for a clearer distinction. (b) The pairwise potential ($U_{\text{Cu,O}}$, the red curve) and force ($F_{\text{Cu,O}} = -\partial U_{\text{Cu,O}}/\partial r_{\text{Cu,O}}$, the blue curve) between the oxygen and solid atoms with respect to the distance ($r_{\text{Cu,O}}$) between them. A positive force on the droplet means “repulsed by the solid,” while a negative one means “attracted by the solid.”

from the initial height of the droplet center of mass to the substrate is

$$H_{\text{ini}} = H_{\text{co}} + r_{\text{cut}} + 10\,000v_i\Delta t + R, \quad (3)$$

where $r_{\text{cut}} = 3.5\sigma_{\text{Cu,O}}$ is the cutoff radius, beyond which the pairwise forces between oxygen and solid atoms are dismissed; v_i is the impact velocity of the droplet; and $\Delta t = 0.001$ ps is the time step of the simulations. Each droplet first experiences sufficient relaxation at 293.15 K using the Nosé-Hoover thermostat, then a vertically downward velocity ranging from 0.5 to 15 Å/ps is applied to the droplet, covering a wide range of Weber numbers from 0.11 to 94.73 and Reynolds numbers from 0.16 to 4.77. In this work, the Weber and Reynolds numbers are defined as $We = \rho v_i^2 R/\gamma$ and $Re = \rho v_i R/\mu$, where ρ , γ , and μ are, respectively, the mass density, surface tension, and dynamic viscosity of the droplet. The surface tension of the initial droplet is evaluated using the Tolman approximation to account for the curvature dependence effects [53,54], and a value of 75.8 mN/m is obtained for a nanodroplet of 32 Å in radius. For the sake of clarity, we also define two near-wall layers: the space below $d = \sqrt[3]{2}\sigma_{\text{Cu,O}}$ of the surface is named as layer 1, where the liquid atoms are repulsed by the solid, while the space between the d and r_{cut} of the surface is named as layer 2, where the liquid atoms are attracted by the solid, as shown in Fig. 1(b).

III. RESULTS AND DISCUSSION

A. Overview of the outcomes

We start by recognizing six typical behaviors of nanodroplets after impacting on the solid surfaces, with the corresponding snapshots shown in Fig. 2. We name them as state 1: deposition; state 2: regular rebound; state 3: impaled

rebound; state 4: ring-ruptured rebound; state 5: film-ruptured rebound; and state 6: breakup. All the states exist on both the flat and cone-textured surfaces except for states 3 and 4, under which the droplet is impaled by the cone to form a ring. The liquid ring then either contracts and rebounds from the cone tip as a whole droplet (state 3), or ruptures to form several subdrops that leave the cone-textured surface radially (state 4). States 5 and 6 occur under high impact velocity conditions, in which the droplet first spreads to form a liquid film, and then holes emerge in the film owing to the larger amplitude of the surface capillary wave than the mean height of the liquid film [42]. The partially ruptured film then either contracts and bounces off the surface as a whole droplet (state 5), or splashes out molecules and finally breaks into pieces (state 6).

With the identification of the six types of droplet behaviors, we plot a panorama of the outcomes in the parameter space of impact velocity and cone geometrics (height and vertex angle), as shown in Fig. 3. Figure 3(a) shows the overall characteristic of each nanocone structure with certain geometrics, while Fig. 3(b) shows how the droplet behaviors change with the impact velocity on each cone geometric. It can be seen that the introduction of nanocone structures generally changes the behavior of the droplet, even when the height of the cone is only one-eighth of the radius of the droplet [cf. the point and column labeled as I in Figs. 3(a) and 3(b)]. Only when the apex angle of the nanocone is close to 180° is the droplet likely to present almost identical behaviors as on the flat surface [cf. the point and column labeled as II in Figs. 3(a) and 3(b)]. Note that a nanocone with an apex angle less than 50°, or with an apex angle of 50° but of height less than 16 Å, cannot be constructed due to limitations of the lattice structure [e.g., the point labeled as III in Fig. 3(a)].

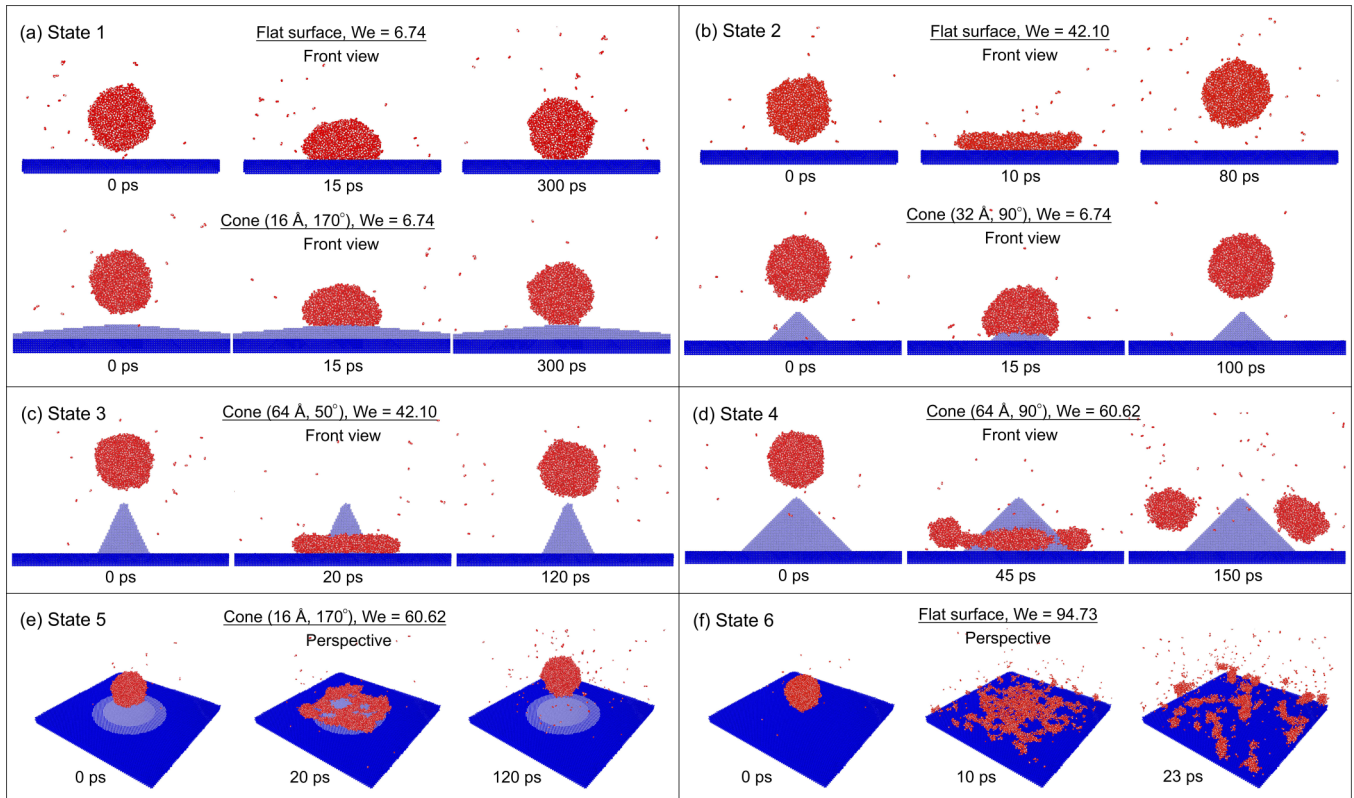


FIG. 2. Snapshots of the six typical behaviors of nanodroplets impacting on solid surfaces: (a) deposition, (b) regular rebound, (c) impaled rebound, (d) ring-ruptured rebound, (e) film-ruptured rebound, and (f) breakup.

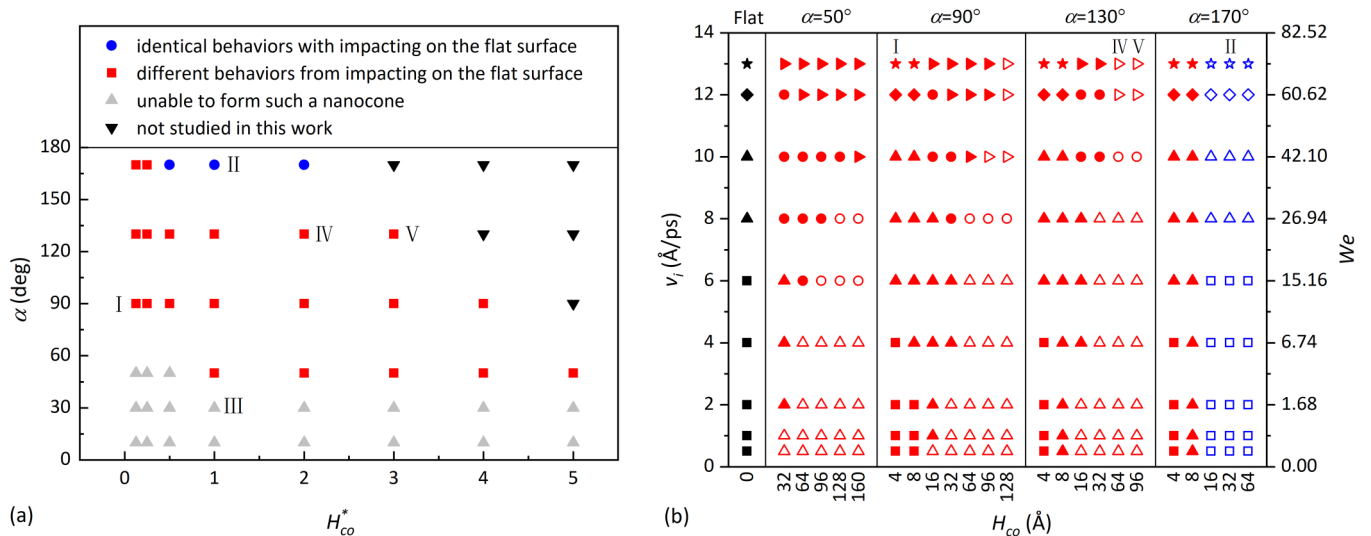


FIG. 3. (a) Phase diagram of the overall characteristics of nanodroplets impacting on the nanocone structures with different geometries (apex angle α and dimensionless height $H_{co}^* = H_{co}/R$). The gray points represent the nanocone geometries that cannot be constructed due to limitations of the lattice structure. The black points correspond to nanocone geometries that are not investigated in this study due to considerations of cone structure self-similarity and computational cost. The red and blue points represent cone structures on which the nanodroplet behaviors are different from, or identical to, those observed on a flat surface (within the scope of impact velocities studied). Each red and blue point in (a) corresponds to a column in (b). (b) Panorama of the outcomes of nanodroplets impacting on flat and nanoconed surfaces, in the parameter space of impact velocity and cone geometries. The square, upward-pointing triangle, circle, right-pointing triangle, diamond, and star symbols represent states 1–6, respectively. Solid or open interior symbols represent the droplet touching or not touching the substrate during impact, respectively.

With the increase of impact velocity, the nanodroplet on the flat surface goes through deposition (state 1), regular rebound (state 2), film-ruptured rebound (state 5), and breakup (state 6), as shown in Fig. 3(b). The introduction of nanocone structures changes the droplet dynamics in the following ways. At low impact velocities, the nanocones promote droplet bouncing, reducing the critical Weber number for rebound from approximately 20 to 0.1 at most; the reasons will be discussed in Sec. III D using momentum analysis. At moderate impact velocities, the introduction of a nanocone changes the droplet behavior from regular rebound (state 2) to impaled rebound (state 3) or ring-ruptured rebound (state 4), and the corresponding changes in restitution coefficient and contact time will be discussed in Sec. III C. At high impact velocities, a nanocone postpones the breakup of the droplet, and this is achieved by changing state 6 to state 4; i.e., the droplet spreads as a liquid ring rather than a thin film on the cone-textured surfaces. Since the rupture of liquids occurs when the amplitude of the surface capillary wave becomes larger than the characteristic scale of the liquid ring or film, and the base circle diameter of the ring is generally larger than the mean height of the film owing to volume conservation, the number of rupture sites in the liquid ring should be less than in the film. As a result, the droplet finally bounces off the cone-textured surfaces in the form of several subdrops, rather than breaking into numerous pieces on the flat surface.

B. Touching or not touching the substrate: A model for the maximum descending height of droplets on nanocone structures

In addition to the previously mentioned six final states, there are two process states that need to be considered, i.e., whether the nanodroplet touches the underlying substrate or not during impact. Hereinafter, we refer to them as “touching states” for convenience. Owing to the self-similarity of cone structures, as long as the droplet does not touch the substrate (or more strictly, never enters the near-wall layers as defined in Fig. 1), the droplet dynamics should only depend on the impact velocity and apex angle, and be independent of the cone height. This is demonstrated in columns labeled as IV and V in Fig. 3(b), where the droplet dynamics on the nanocones with an apex angle of 130° remains the same despite the increase in cone height from 64 to 96 Å. By examining the touching states, we can eliminate the influence of cone height, which can simplify theoretical analysis and facilitate industrial design.

It can also be seen in Fig. 3(b) that increasing the impact velocity enables the droplets to touch the substrate, while increasing the apex angle of the cones prevents the droplets from touching the substrate. To investigate the quantitative relations between the touching states and the impact velocity, as well as the apex angle of nanocone structures, we define the descending height of a droplet on such structures (h_d) as the vertical distance from the lowest point of the droplet surface to the tip of the cone, and examine the maximum descending height of the droplet during the complete impact process ($h_{d,\max}$). For state 1, $h_{d,\max}$ refers to the descending height at which the droplet comes to rest after impact. For states 2–5, $h_{d,\max}$ denotes the descending height at which the vertical

velocity of the droplet (or subdrops in state 4) decelerates to zero, just before rebound. State 6 has been excluded from our analysis due to its unclear definition for $h_{d,\max}$.

As shown in Fig. 4(a), the dimensionless maximum descending height ($h_{d,\max}^* = h_{d,\max}/R$) varies with the impact velocity and apex angle as expected, with a fitted relation,

$$h_{d,\max}^* \tan(\alpha/2) = (0.33 \pm 0.04) \text{We}^{0.45 \pm 0.04}, \quad (4)$$

$$\text{We} \in (0.1, 100),$$

holding for all the final states except for state 4 (ring-ruptured rebound). Since $h_{d,\max}^* \tan(\alpha/2)$ also characterizes the spreading dynamics of droplets on the cone structures, and the scaling law of $\text{We}^{0.45}$ is between the $\text{We}^{1/4}$ law for the no-slip surfaces and the $\text{We}^{1/2}$ law for the free-slip surfaces [55], it is indicated that the spreading of droplets on the conical inclined surface is akin to partial-slip walls. Using this semiempirical relation and the definition of a droplet not touching the substrate (the droplet never enters the near-wall layers, i.e., $h_{d,\max} + r_{\text{cut}} < H_{\text{co}}$), we obtain the condition for the untouched state:

$$H_{\text{co}}^* > \frac{\text{We}^{0.45}}{3 \tan(\alpha/2)} + \frac{r_{\text{cut}}}{R}. \quad (5)$$

As shown in Fig. 4(b), Eq. (5) accurately predicts the range of parameters in which a nanodroplet does not touch the substrate, except for a few cases corresponding to state 4. For state 4, the subdrops generated from the rupture of the liquid ring can slide down and along the inclined conical surface, resulting in a sharp increase in the maximum descending height.

In order to better understand the conditions under which Eq. (5) fails, it is necessary to investigate the critical descending height ($h_{d,\text{cr}}$) at which the liquid ring ruptures. Consider a nanodroplet impaled by the cone to form a liquid ring, as shown in Fig. 5(a), and note that this liquid ring is not of equal section owing to the generation and growth of the surface capillary waves [56]. The capillary waves loop through the liquid ring, resulting in the radius of the ring section fluctuating between r at the trough and n times r at the crest. The average cross-sectional area of the liquid ring can be estimated by approximating it as a series of conical frustums spliced together, which yields a value of

$$\bar{S} \approx \frac{1}{3} \pi [(nr)^2 + nr(r) + r^2] = \frac{\pi}{3} (n^2 + n + 1)r^2. \quad (6)$$

The average distance from the center of the ring section to the axis of the ring is approximately

$$\bar{c} \approx 0.5(c_1 + c_2), \quad (7)$$

where

$$c_1 = h_d \tan \frac{\alpha}{2} + nr \tan \psi, \quad (8)$$

$$c_2 = [h_d - (n-1)r] \tan \frac{\alpha}{2} + r \tan \psi, \quad (9)$$

$$\psi = \frac{1}{2} \left(\frac{\pi}{2} - \frac{\alpha}{2} \right). \quad (10)$$

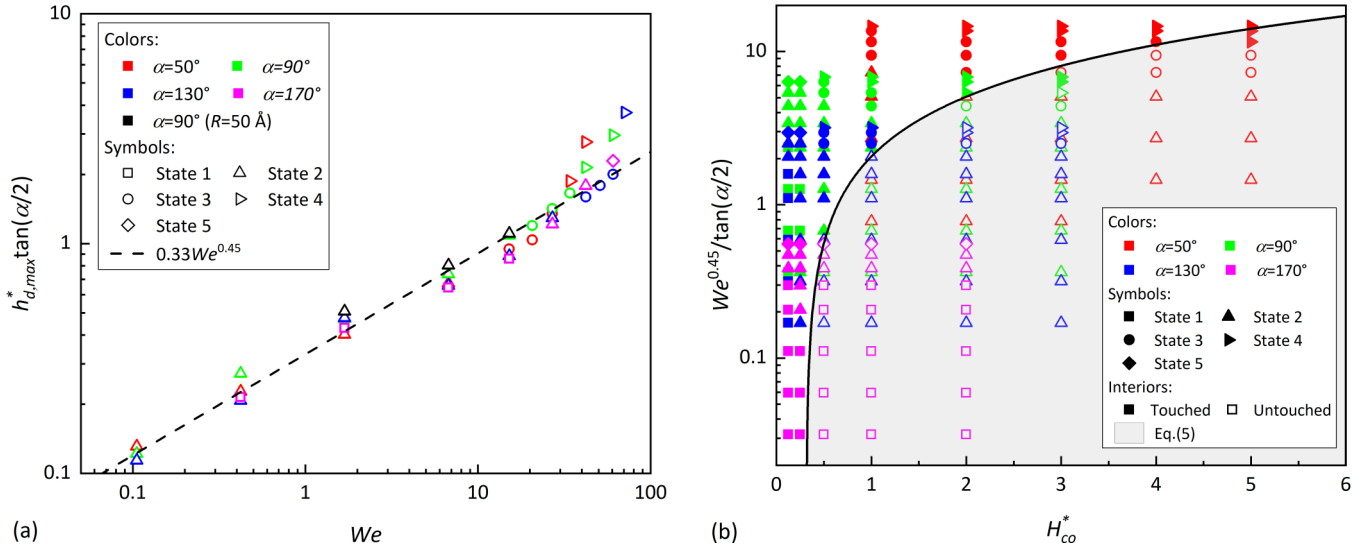


FIG. 4. (a) The dimensionless maximum descending height of the nanodroplet with respect to the Weber number and apex angles. The nanocones are large enough to ensure that the droplets do not touch the substrate during impact. (b) Phase diagram of the nanodroplet in the parameter space of dimensionless cone height and $We^{0.45}/\tan(\alpha/2)$. The black curve predicts the boundary between two touching states except in a few cases of state 4.

The volume of the liquid ring then sets to

$$V_{\text{ring}} = \bar{S}2\pi\bar{c}, \quad (11)$$

which is equal to the initial volume of the nanodroplet owing to volume conservation, that is,

$$V_0 = \frac{4\pi}{3}R^3. \quad (12)$$

With Eqs. (6)–(12), we obtain the expression for the dimensionless descending height of an impaled nanodroplet as

$$h_d^*(\alpha) = \frac{h_d(\alpha)}{R} = \frac{2}{(n^2 + n + 1)\pi \tan(\alpha/2)} \left(\frac{R}{r}\right)^2 + \left[n - \frac{n+1}{2 \sin(\alpha/2)} \right] \left(\frac{r}{R}\right). \quad (13)$$

From the microscopic perspective, a liquid ring can be considered ruptured if the radius of the ring section at the trough

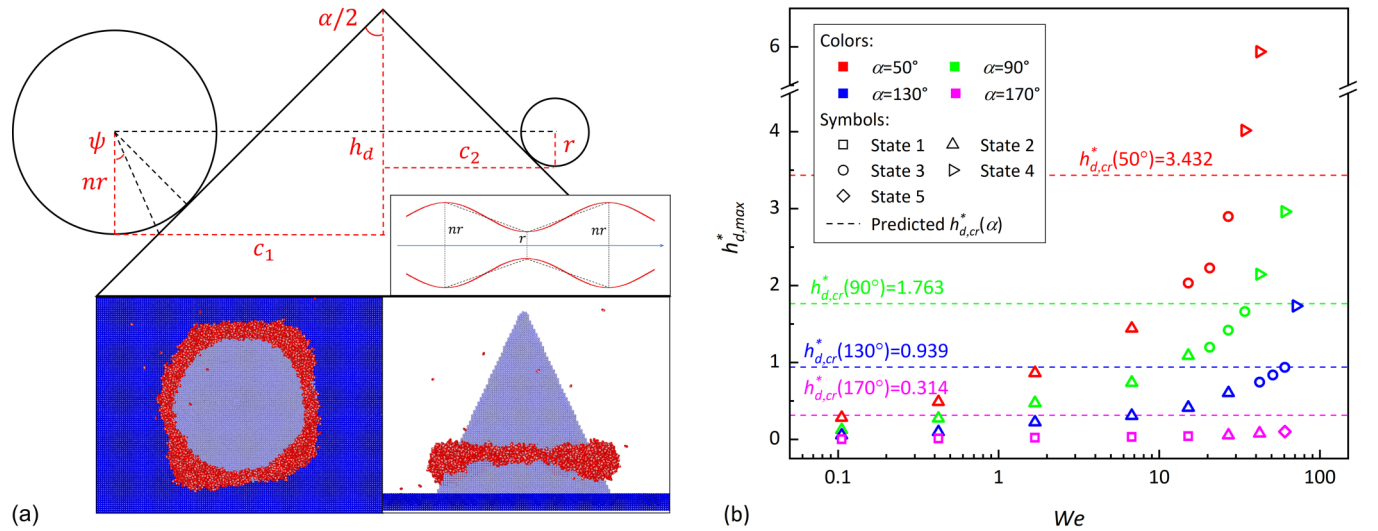


FIG. 5. (a) Schematic diagram of a liquid ring formed by an impaled droplet on the nanocone structure. Below the schematic diagram are typical snapshots from top and front views when the liquid ring is about to rupture. (b) The dimensionless maximum descending height and the predicted critical descending heights of the droplet on various nanocone structures. If $h_{d,max}^* > h_{d,cr}^*$, the liquid ring will rupture, manifested as state 3 changing to state 4.

(r) approaches $r_{\text{cut},O}/2$, where $r_{\text{cut},O} = 3.5\sigma_O$ is the range of action of intermolecular forces between water molecules, whose value actually measures the thickness of the liquid surface [42]. As a result, the critical descending height when the liquid ring is about to rupture can be calculated via

$$h_{d,\text{cr}}^*(\alpha) = \frac{8}{(1 + 1/n + 1/n^2)\pi \tan(\alpha/2)} + \left[\frac{1}{2} - \frac{1 + 1/n}{4 \sin(\alpha/2)} \right], \quad (14)$$

where we have used an approximation of $n \sim R/r_{\text{cut},O}$. As shown in Fig. 5(b), Eq. (14) accurately predicts the boundary between states 3 and 4. This implies that if the descending height of an impaled nanodroplet surpasses this critical value during impact, the liquid ring will rupture and the relations described by Eqs. (4) and (5) will no longer hold. We note that a complete modeling of n would need to take into account the growth of Rayleigh-Plateau instability coupled with thermal fluctuations [57], which is challenging due to the average radius of the liquid ring varying with time as the liquid ring descends and spreads on the cone structures. Fortunately, Eq. (14) is not highly dependent on the value of n when it exceeds 3, which is applicable to the majority of practical cases.

C. Pros or cons of the nanocone structures: In terms of the restitution coefficient and contact time

In Sec. III A, we showed that nanocone structures promote bouncing at low impact velocities and postpone breakup at high impact velocities. At moderate impact velocities, the droplet rebounds from both the flat surface and the cone-textured surface, and thus the effects of the nanocone structure need to be further investigated. The restitution coefficient and contact time are two of the most used properties to evaluate the bouncing performance of a droplet. Therefore, in this section, we compare these two properties of nanodroplets on the flat surface with those on the cone-textured surfaces, where nanocone structures of height 64 \AA are used as the example.

The values of restitution coefficient may vary depending on the specific procedures employed to determine the rebound velocity. Our approach involves calculating the velocity of a nanodroplet by averaging the velocity of all water molecules that remain in the droplet (or in any subdrops when the droplet fragments) during impact. The rebound velocity is then measured once the nanodroplet (or all subdrops) have bounced off the surface and left the near-wall layers. In this context, the measured velocity should be time independent due to the cutoff of solid-liquid intermolecular forces and the negligible effects of gravity (the Froude number $\text{Fr} = v/\sqrt{gR} \gg 1$, where g is the gravitational acceleration). However, some small fluctuations may occur in the velocity due to the long-range interactions and numerical disturbances. To account for this, we take an average of the rebound velocity over thousands of time steps and use the resulting value to calculate the restitution coefficient.

As shown in Fig. 6(a), the restitution coefficient of a nanodroplet on cone-textured surfaces presents two distinct changing rules, marked by whether the liquid ring ruptures. For the nonruptured rebound regimes (i.e., states 2 and 3), the restitution coefficient on cone-textured surfaces generally decays with the Weber number, but is consistently larger than on the flat surface. A qualitative explanation for this might be that there is less viscous dissipation on cone-textured surfaces owing to the partial-slip characteristics of the conical inclined surface, as discussed in Sec. III B. In these regimes, the restitution coefficient can be fitted as

$$\beta_v [\tan(\alpha/2)]^{0.5} = (0.25 \pm 0.02) \text{We}^{-0.25 \pm 0.04}, \quad \text{We} \in (0.1, 30), \quad (15)$$

as depicted in Fig. 6(b), providing practical value for the designs of nanocone structures. For state 4, nevertheless, the restitution coefficient on cone-textured surfaces decreases sharply to a value below that found on the flat surface. In this regime, a nanodroplet splits into several subdrops, and the increase in the surface energy can lead to a decrease in the kinetic energy for rebound. Since a large restitution coefficient is commonly expected to facilitate collection and discharge of the droplets, it is overall beneficial to introduce the nanocone structure on the flat surface, while the impact velocity range that gives rise to state 4 should be avoided.

Regarding the contact time, there is more than one reasonable definition at the nanoscale [36,58]. In this work, we define the ‘‘contact’’ as there being at least 8 ($\approx 0.5\sqrt[3]{4582}$) oxygen atoms located inside the near-wall layers. Such a definition conforms to the nature of contact, i.e., the mass, momentum, and energy transfers between the droplet and surface. The contact time measured using this definition is presented in Fig. 6(c) (note that the contact time has been normalized by the inertial-capillary timescale, i.e., $\tau_c^* = \tau_c/\sqrt{\rho R^3/\gamma}$ [59]). Three interesting phenomena can be found from the results. First, with increased Weber number, the dimensionless contact time on cone-textured surfaces initially decreases and then increases, and the Weber number at which the contact time is minimum is inversely related to $\tan(\alpha/2)$, as shown in the inset of Fig. 6(c). Second, for the droplets with the same Weber number, despite the smaller restitution coefficient on blunter nanocone structures (i.e., with a larger apex angle), the contact time on such cone-textured surface is also smaller. Third, contrary to our intuition, the contact times of nanodroplets on cone-textured surfaces are larger than on the flat surface in most of the cases.

To explain these phenomena, we divide the whole impact-rebound process of the droplets into four stages, namely, stage 1 (from entering the near-wall layers to touching the flat surface or cone tip), stage 2 (spreading on the flat surface or descending along the cone structure), stage 3 (retracting on the flat surface or lifting along the cone structure), and stage 4 (from detaching from the flat surface or cone tip to leaving the near-wall layers), and measure the duration of each stage. As shown in Fig. 6(d), the large contact time at low impact velocities is mainly attributable to the long duration of falling and rising through the near-wall layers (i.e., stages 1 and 4). At large impact velocities, despite the very short duration of stage 1, stage 4 still takes a long period of time owing to the very

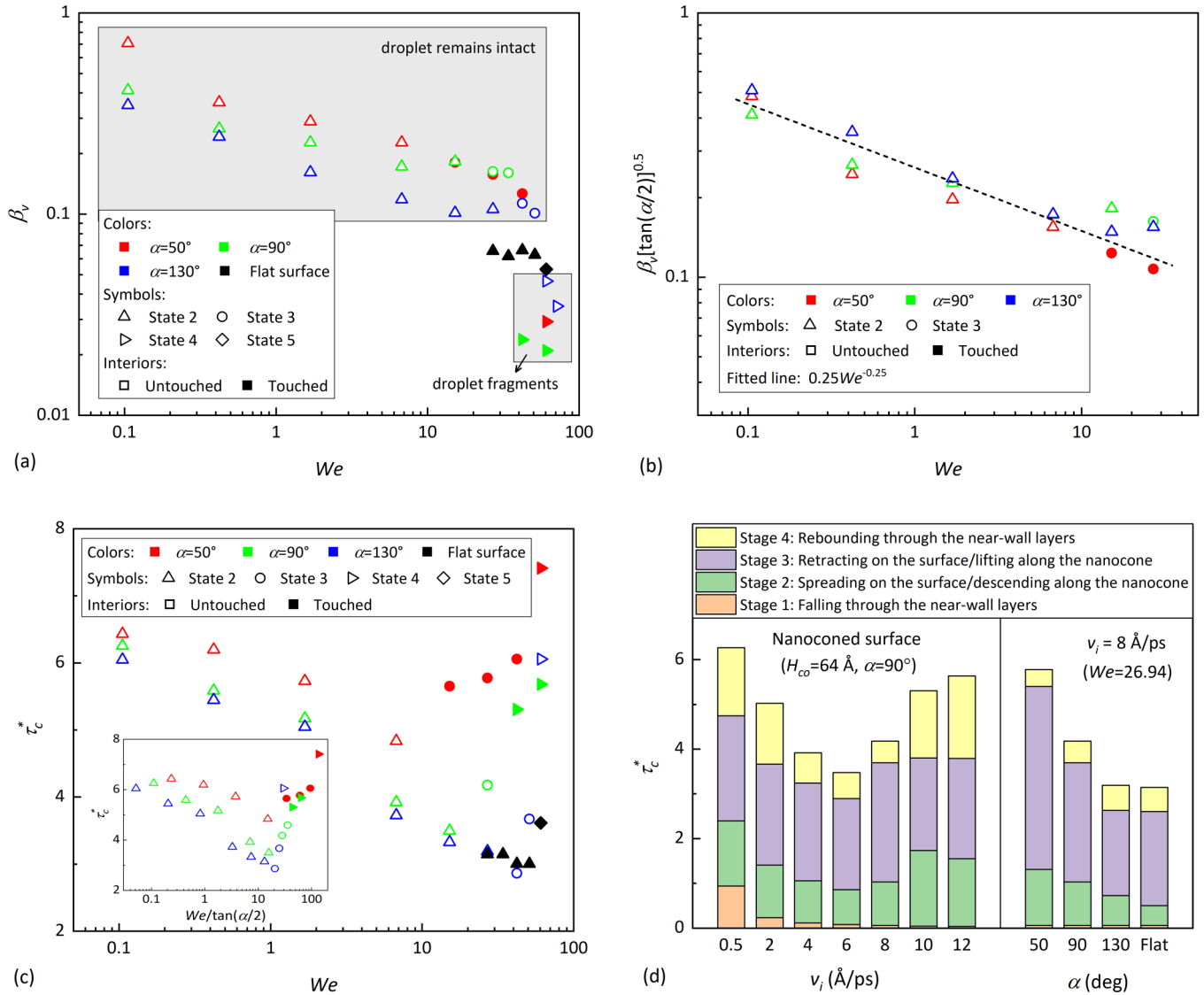


FIG. 6. (a) The restitution coefficient, (c) dimensionless contact time, and (d) duration of each stage in the impact-rebound process of nanodroplets that impact on the flat surface or on cone-textured surfaces with the cone height of 64 Å. (b) The fitted relation for the restitution coefficient of nanodroplets that rebound from the cone-textured surfaces in the nonruptured regimes.

small restitution coefficient and thus lower rebound velocity. As a result, it is at the moderate impact velocities that the contact time reaches a minimum. For the nanodroplets with the same Weber number, as the apex angle of the nanocone increases, it is obvious that the duration of stage 1 remains the constant, while the duration of stage 4 increases owing to the smaller restitution coefficient resulting from the blunter cone structures—the decrease in the total contact time at the blunter nanocones is essentially originated from stages 2 and 3, as the maximum descending height of nanodroplets along the nanocone structures is negatively correlated with the apex angle [cf. Eq. (4)]. This also explains why the contact time on the flat surface, which can be regarded as a “cone” of $\alpha = 180^\circ$, is smaller than most of the nanocone cases. Therefore, introducing nanocone structures to the surface avails applications that require heat and mass transfers such as cooling, but is detrimental to those with opposite purposes such as anti-icing.

D. How nanocones promote bouncing: Forces and momentum analysis in nanodroplets impact

In Sec. III A, we mention that the introduction of nanocone structures enables nanodroplets with low impact velocities to bounce off, rather than deposit on the surface. In the following, we discuss this phenomenon from the perspective of momentum analysis rather than the classical energy analysis, given that the forces exerted on the droplet by the solid surface can be directly calculated in MD simulations via

$$\begin{aligned}
 F_z &= \sum -\frac{\partial}{\partial z} U_{\text{Cu,O}} \\
 &= -4\xi_{\text{Cu,O}} \sum_{i \in \text{oxygen}} \sum_{j \in \text{solid}} \frac{\partial}{\partial z} \left[\left(\frac{\sigma_{\text{Cu,O}}}{r_{ij}} \right)^{12} - \left(\frac{\sigma_{\text{Cu,O}}}{r_{ij}} \right)^6 \right],
 \end{aligned} \tag{16}$$

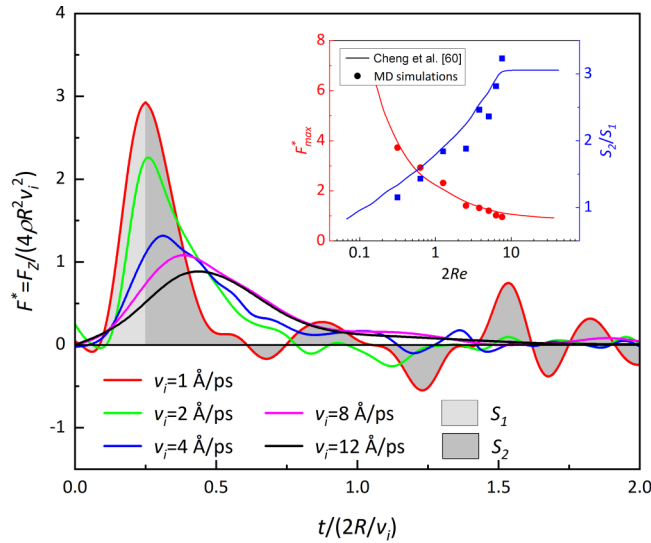


FIG. 7. The temporal evolution of the dimensionless intermolecular forces exerted by solid atoms on the nanodroplet as it impacts on the flat surface at varying velocities. The S_1 and S_2 values correspond to the area of the force curve integrated over time before and after the peak force, respectively. Note that the intermolecular force can be negative, indicating an overall attraction between the droplet and the surface. The inset compares the dimensionless force peak and the area ratio S_2/S_1 of the impacting nanodroplet to the trend lines reported at the macroscale [60], and note that the x -coordinate variable is $2Re$ because we define the Reynolds number using the droplet radius instead of the diameter used in the literature [60].

where a negative or positive value signifies the attractive or repulsive force, respectively. Figure 7 depicts the temporal evolution of the measured intermolecular forces that solid atoms exert on the nanodroplet as it impacts on the flat surface

at various velocities. The qualitative features of this evolution are similar to those reported at the macroscale [60], where the impact forces rise quickly, and then decay over a longer period after they reach the maximum, resulting in an asymmetric force-time curve with respect to the peak force. The inset in Fig. 7 demonstrates that the dependencies of characteristic quantities of solid-liquid intermolecular forces on the Reynolds number exhibit remarkable similarity to those of the impact force observed at the macroscale [60], which further confirms the reliability of our calculations.

Figure 8(a) shows the temporal evolution of the solid-liquid intermolecular forces and the resulting impulse on the nanodroplet with an impact velocity of 4 \AA/ps . This velocity is a good example of a scenario in which the nanodroplet will deposit on the flat surface, but bounce off the cone-textured surfaces. Generally, there are two reasons to account for this discrepancy. First, despite the smaller first force peak, the droplet experiences a greater upward impulse on the cone-textured surface compared to the flat surface, owing to the longer duration of the repulsive force, as shown in Fig. 8(a). To investigate this phenomenon, we compare the number of water molecules inside the repulsive layer over time, as shown in Fig. 8(b). We observe that when a nanodroplet impacts on the flat surface, the center of mass reaches its minimum height (t_1) prior to the maximum spreading time (t_2) (cf. the inset in Fig. 8(b) and more evidence in Refs. [61,62]). It is not our focus to further discuss the reasons for $t_1 < t_2$, but we note that the droplet lifting prior to retracting leads to the number of water molecules in layer 1 rapidly decreasing. These remaining molecules experience insufficient repulsive forces to balance the attractive forces acting on the water molecules in layer 2, causing the droplet to eventually deposit on the surface. In contrast, the presence of a nanocone structure allows the droplet to cling to the solid surface during retraction

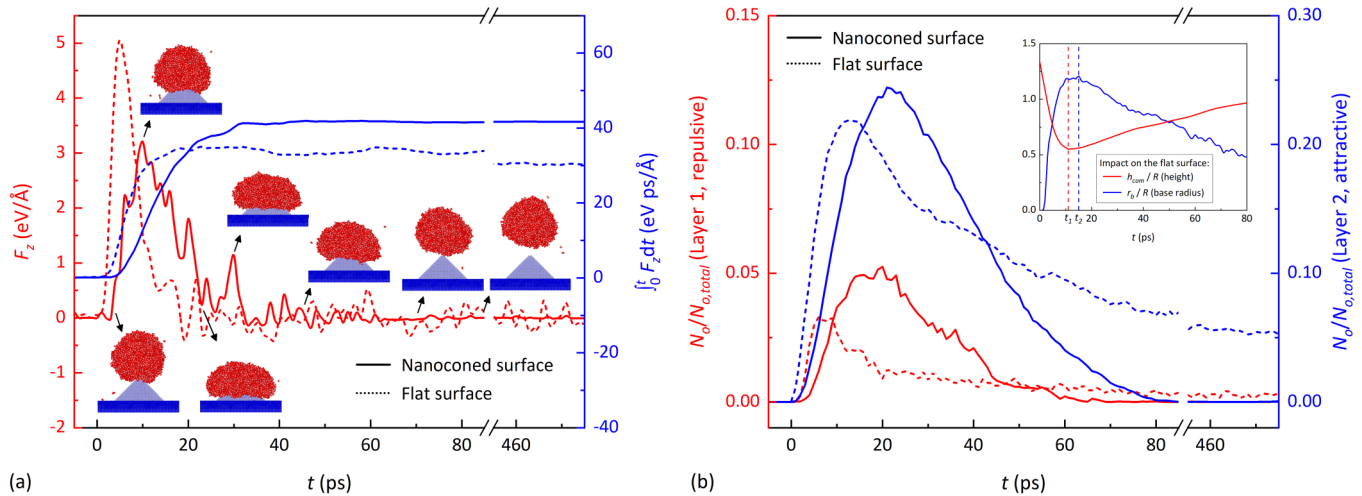


FIG. 8. Nanodroplet of 4 \AA/ps eventually deposits on the flat surface but bounces off the nanoconed surface ($H_{co} = 32 \text{ \AA}$, $\alpha = 90^\circ$). (a) The forces and impulse on the nanodroplet exerted by the solid surfaces. The chronologically displayed snapshots depict characteristic instants of the nanodroplet on the cone-textured surface, including initial contact with the cone tip, the first force peak during spreading, maximum spreading, the second force peak during retraction, maximum upward impulse with solid-liquid intermolecular forces initially fluctuating around zero, detachment from the cone tip, and departure from the near-wall layer. (b) Ratio of the number of oxygen atoms inside the near-wall layers to the total oxygen atoms. The inset shows the temporal evolution of the base radius and the height of the center of mass of the nanodroplet impacting on the flat surface.

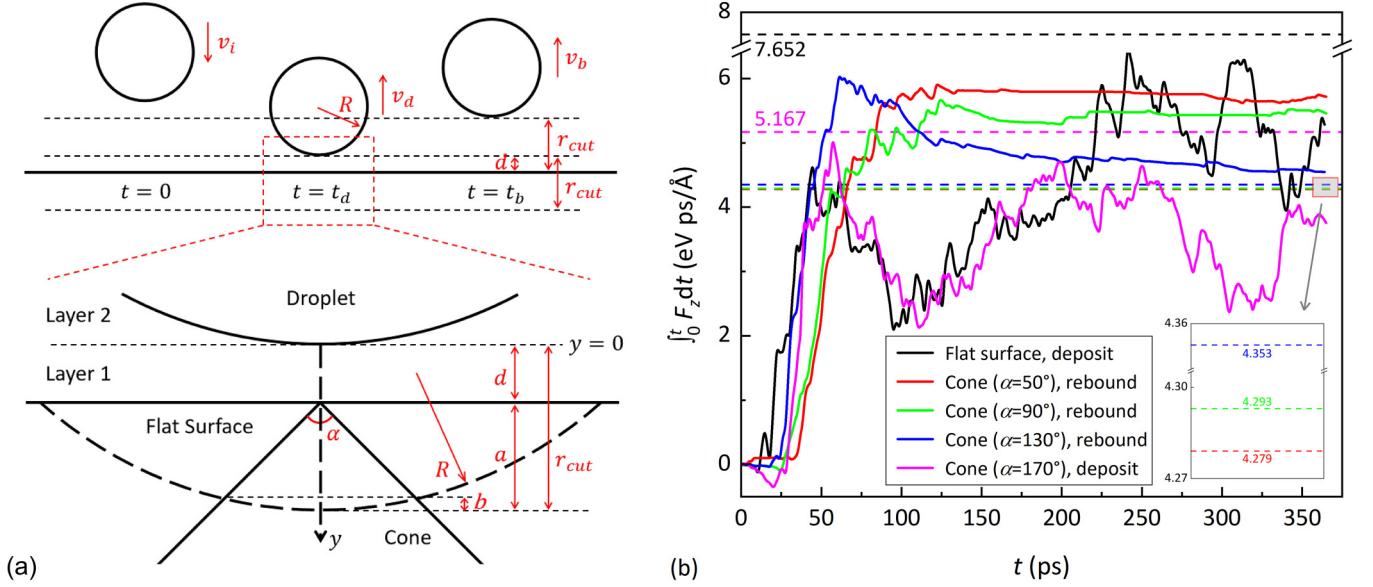


FIG. 9. (a) Schematic diagram of a nanodroplet that has just departed from layer 1. The long black dashed line approximates the farthest limit at which a solid atom can interact with the droplet (if not considering the long-range forces). (b) The measured impulse on the nanodroplet exerted by the solid atoms (solid lines) and the predicted critical impulse for rebound (dashed lines). The impact velocity of the nanodroplet is 0.5 \AA/ps .

and lifting, maintaining 1%–5% of the water molecules within layer 1 until the droplet gains the upward impulse required for bouncing off the surface.

Two other intriguing phenomena shown in Fig. 8(a) are worth mentioning. Firstly, the second force peak of the nanodroplet during retraction is less prominent than that observed in the macroscale situation [63], as the singular cavity collapse may not occur at the nanoscale where the Ohnesorge number is typically $\text{Oh} = \mu/\sqrt{\rho\gamma R} = O(1)$. Secondly, as the nanodroplet rises to the upper half of the nanocone (well before the droplet detaches from the cone tip or leaves the near-wall layers), the overall solid-liquid intermolecular

forces become insignificant, despite there still being over 5% of the water molecules present within layer 2 [cf. Fig. 8(b)]. This phenomenon indicates the second reason why nanocones can promote bouncing, namely, the reduced adhesion effect of cone-textured surfaces compared to the flat surface.

To further illuminate this, consider a nanodroplet that has just departed from layer 1 to cross layer 2, where the distance from the bottom of the droplet to the flat surface or cone tip is d , as depicted in Fig. 9(a). We neglect the oscillation of the droplet and assume it remains spherical; then the ratio of the attractive force exerted on the droplet by the nanocones and flat surface is estimated as

$$\eta \approx \frac{\int_d^{d+a-b} \frac{R}{y^3} \rho_s \pi [(y-d) \tan \frac{\alpha}{2}]^2 dy + \int_{d+a-b}^{d+a} \frac{R}{y^3} \rho_s \pi [R^2 - (R-d-a+y)^2] dy}{\int_d^{d+a} \frac{R}{y^3} \rho_s \pi [R^2 - (R-d-a+y)^2] dy} = \frac{\tan^2 \frac{\alpha}{2} \left(-\frac{1}{2y^2} + \frac{2d}{3y^3} - \frac{d^2}{4y^4} \right) \Big|_d^{d+a-b} + \left[\frac{1}{2y^2} - \frac{2(d+a-R)}{3y^3} - \frac{(d+a)(2R-d-a)}{4y^4} \right] \Big|_{d+a-b}^{d+a}}{\left[\frac{1}{2y^2} - \frac{2(d+a-R)}{3y^3} - \frac{(d+a)(2R-d-a)}{4y^4} \right] \Big|_d^{d+a}}, \quad (17)$$

where Ry^{-5} is the approximate scaling law for the van der Waals force between a sphere and a molecular, ρ_s is the number density of solid molecules, and the two geometric parameters a and b are calculated via

$$a = r_{\text{cut}} - d, \quad (18)$$

$$\left[(a-b) \tan \frac{\alpha}{2} \right]^2 + (R-b)^2 = R^2. \quad (19)$$

The results give $\eta \approx 0.12\%$, 0.55% , 2.30% , and 26.41% for $\alpha = 50^\circ$, 90° , 130° , and 170° , respectively. We observe that the attractive force from most of the cone-textured sur-

faces is almost negligible compared to that of the flat surface, and even a cone structure of $\alpha = 170^\circ$ reduces the attractive force on the droplet by 75%. This reduction in adhesion is most notable for those nanodroplets with small impact velocities, as the condition for a nanodroplet to bounce off the surface can be expressed as

$$I_d = \int_0^{t_d} F_z dt \geq I_{d,\text{cr}} \approx m(v_i + \eta v_{d,\text{min}}), \quad (20)$$

where $I_{d,\text{cr}}$ is the critical impulse for rebound, and $v_{d,\text{min}}$ is the minimum speed required for the droplet to cross through

layer 2 on the flat surface. It can be seen from Eq. (20) that the second term will make an equivalent contribution to the critical impulse when the impact velocity is small. Therefore, a small η significantly decreases the value of $I_{d,cr}$, which makes it possible for the nanodroplets even with considerably low Weber number to rebound (note that $\eta = 1$ for the flat surface).

Due to the negligible effects of gravity on the nanodroplet, the value of $v_{d,min}$ can be estimated via

$$\frac{1}{2}mv_{d,min}^2 \approx \frac{A_H R}{6} \left(\frac{1}{d} - \frac{1}{r_{cut}} \right) + \frac{1}{2}mv_b^2 \Big|_{v_b=0}, \quad (21)$$

where A_H is the Hamaker constant, approximately corresponding to the geometric mean of the values for water-water and copper-copper interactions that can be found in [64,65]. Using Eqs. (17)–(21), one can calculate the critical impulse required for a nanodroplet with a certain impact velocity to rebound, and this can be directly verified by measuring the vertical force exerted on the droplet by the solid atoms. An example is shown in Fig. 9(b), where the nanodroplet of $v_i = 0.5 \text{ \AA/ps}$ requires an impulse larger than 7.652 eV ps/\AA to rebound from the flat surface, while on the cone-textured surfaces with apex angles of 50° , 90° , and 130° , the value decreases to 4.279 , 4.293 , and 4.353 eV ps/\AA , respectively. As a result, the droplet deposits on the flat surface, while it successfully rebounds from these three kinds of cone-textured surfaces.

E. Links between nanodroplets and millimeter-sized droplets: Beyond the Weber number

Finally, we discuss the links between nanodroplets and millimeter-sized droplets, where a single Weber number is not adequate to unify their dynamics, as clarified in Sec. I. A similar phenomenon can be observed in a droplet impacting on cone-textured surfaces, where the critical Weber numbers for nanodroplets to experience “impaled rebound” or “ring-ruptured rebound” from cone structures are significantly higher than those for millimeter-sized droplets, as depicted in Fig. 10(a). This suggests that the nanodroplets require a much larger Weber number to exhibit equivalent inertia effects as the millimeter-sized droplets, possibly because of the amplified effects of viscous and solid-liquid intermolecular forces at the nanoscale. To further illustrate this, we define two dimensionless numbers to describe the relative magnitudes of adhesion and dissipation to the inertia of a droplet during the impact process,

$$\phi_{a,i} = \frac{E_{ad}}{E_k} = \frac{A_H R / 6d}{2\pi\rho R^3 v_i^2 / 3} = \frac{A_H}{4\pi\gamma d} \frac{1}{RWe}, \quad (22)$$

$$\begin{aligned} \phi_{v,i} &= \frac{E_v}{E_k} = \frac{\pi\mu R^2 v_i (\beta_{max}^2 - 2/3)}{2\pi\rho R^3 v_i^2 / 3} \\ &= \frac{\mu(3\beta_{max}^2/2 - 1)}{\sqrt{\rho\gamma}} \frac{1}{\sqrt{RWe}}, \end{aligned} \quad (23)$$

where the adhesion energy (E_{ad}) is estimated via the work done by the droplet to overcome the attractive force exerted by the solid atoms in leaving the surface, the viscous dissipation (E_v) is expressed via the acknowledged model proposed by Li

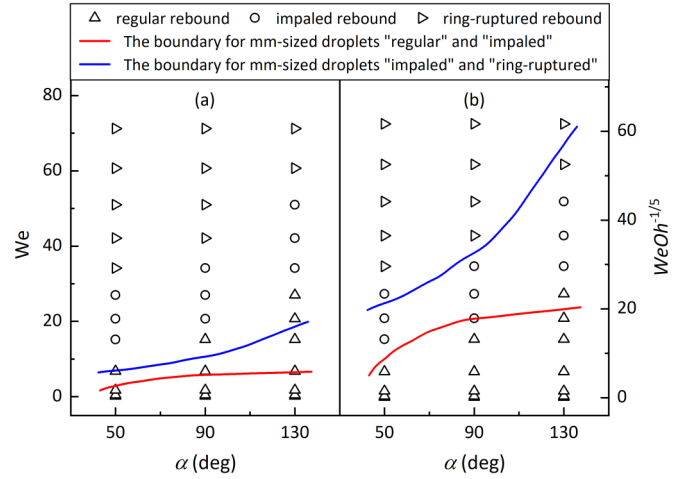


FIG. 10. The droplet behaviors after impacting on the cone structures. The symbols are the MD simulation results of the nanodroplets, while the solid lines are extracted from the work of Luo *et al.* [46] who studied millimeter-sized droplets.

et al. [41], and the kinetic energy (E_k) is calculated via the impact velocity of the droplet. It can be seen that $\phi_{a,i}$ and $\phi_{v,i}$ for the nanodroplets will be orders of magnitude larger than for their macroscopic counterparts despite having the same Weber number [note that $\beta_{max} = O(1)$ at both scales]. Therefore, droplets with the same Weber number, but of different scales, present different dynamics.

Equations (22) and (23) can be further rewritten as

$$\phi_{a,i} = \frac{A}{We}, \quad (24)$$

$$\phi_{v,i} = \frac{Oh}{\sqrt{We}} (3\beta_{max}^2/2 - 1), \quad (25)$$

where $A = A_H / 4\pi\gamma dR$. This indicates that to compare the dynamics of droplets of different sizes, it is essential to consider a combination of dimensionless numbers that incorporate the A , We , Oh , and β_{max} to accurately describe the relative roles of adhesion, capillary, viscosity, and inertia at different scales. Among these effects, adhesion plays a less important role on cone-textured surfaces, as explained in Sec. III D. Besides, the maximum spreading factor has analytical solutions in the forms of $\beta_{max} = f(We, Re)$ [20,26] or $\beta_{max} = f(We, Ca)$ [12], where $Ca = \mu v_i / \gamma$ is the capillary number, and it should be noted that only two of these dimensionless parameters (We , Oh , Re , and Ca) are independent [66]. As a result, the anticipated combined dimensionless number is primarily expressed in terms of We and Oh , i.e., $Q = WeOh^x$, where x is the undetermined exponent. As shown in Fig. 10(b), we observe that the dynamics of nanodroplets and millimeter-sized droplets can be well unified in the framework of such a combined dimensionless number with $x = -1/5$. This enables the prediction of droplet behaviors, such as whether a droplet will undergo “regular rebound,” “impaled rebound,” or “ring-ruptured rebound” from cone structures—once the number Q has been determined—regardless of the droplet scales. This approach shows promise for studying the multiscale dynamics of droplet impacts, and constructing a corresponding combined dimensionless number for other kinds of textured

surfaces should be similar. Developing a universal scaling law for the number Q (essentially, developing a universal model for evaluating the exponent x) would be a valuable issue for the future.

IV. CONCLUSIONS

In this work, we performed molecular dynamic simulations to study the dynamics of nanodroplets impacting on a flat superhydrophobic surface and cone-textured surfaces. The main conclusions are as follows.

(1) There exist six typical final states (i.e., deposition, regular rebound, impaled rebound, ring-ruptured rebound, film-ruptured rebound, and breakup) and two process states (i.e., touching and not touching the underlying substrate during the impact process) for a nanodroplet impacting on the cone-textured surfaces. A model that accurately predicts the process states of nanodroplets is developed.

(2) Introducing even a tiny cone with the height as small as one-eighth the radius of the nanodroplet to the flat substrate can change the droplet dynamics. The introduction of nanocone structures generally promotes bouncing at low

impact velocities, postpones breakup at high impact velocities, and facilitates an increased restitution coefficient, but is detrimental in reducing contact time.

(3) The nanocone structures enhance bouncing by increasing the upward impulse that a nanodroplet gains from the solid surface due to the longer duration of repulsive force, and by reducing the critical upward impulse required for a nanodroplet to rebound due to the decreased adhesion of the surfaces. A momentum-analysis-based model is developed to describe the effects of nanocone structures on the droplet bouncing dynamics.

(4) The impact dynamics of the nanoscale and macroscale droplets cannot be unified by a single Weber number owing to the larger contribution of adhesion and dissipation effects at the nanoscale. A combined dimensionless number, i.e., $Q = \text{WeOh}^{-1/5}$, is proposed to link the dynamics of droplets with different scales that impact on the cone structures.

ACKNOWLEDGMENT

This work was supported by the National Natural Science Foundation of China (Grant No. 92052104).

-
- [1] J. Hengsteler, B. Mandal, C. van Nesselroy, G. P. S. Lau, T. Schlotter, T. Zambelli, and D. Momotenko, Bringing electrochemical three-dimensional printing to the nanoscale, *Nano Lett.* **21**, 9093 (2021).
- [2] W. Wu, H. Bostanci, L. C. Chow, S. J. Ding, Y. Hong, M. Su, J. P. Kizito, L. Gschwender, and C. E. Snyder, Jet impingement and spray cooling using slurry of nanoencapsulated phase change materials, *Int. J. Heat Mass Transfer* **54**, 2715 (2011).
- [3] A. Ishijima, K. Minamihata, S. Yamaguchi, S. Yamahira, R. Ichikawa, E. Kobayashi, M. Iijima, Y. Shibasaki, T. Azuma, T. Nagamune *et al.*, Selective intracellular vaporisation of antibody-conjugated phase-change nano-droplets *in vitro*, *Sci. Rep.* **7**, 44077 (2017).
- [4] J. Zhang, M. K. Borg, and J. M. Reese, Multiscale simulation of dynamic wetting, *Int. J. Heat Mass Transfer* **115**, 886 (2017).
- [5] J. Zhang, P. F. Wang, M. K. Borg, J. M. Reese, and D. S. Wen, A critical assessment of the line tension determined by the modified Young's equation, *Phys. Fluids* **30**, 082003 (2018).
- [6] A. S. Rana, D. A. Lockerby, and J. E. Sprittles, Lifetime of a Nanodroplet: Kinetic Effects and Regime Transitions, *Phys. Rev. Lett.* **123**, 154501 (2019).
- [7] T. Zhang, F. Javadpour, X. Li, K. Wu, J. Li, and Y. Yin, Mesoscopic method to study water flow in nanochannels with different wettability, *Phys. Rev. E* **102**, 013306 (2020).
- [8] H. Liu, J. Zhang, P. Capobianchi, M. K. Borg, Y. Zhang, and D. Wen, A multiscale volume of fluid method with self-consistent boundary conditions derived from molecular dynamics, *Phys. Fluids* **33**, 062004 (2021).
- [9] M. Heiranian and N. R. Aluru, Modified Lucas-Washburn theory for fluid filling in nanotubes, *Phys. Rev. E* **105**, 055105 (2022).
- [10] P. Galliker, J. Schneider, H. Eghlidi, S. Kress, V. Sandoghdar, and D. Poulikakos, Direct printing of nanostructures by electrostatic autofocussing of ink nanodroplets, *Nat. Commun.* **3**, 890 (2012).
- [11] S. Mura, J. Nicolas, and P. Couvreur, Stimuli-responsive nanocarriers for drug delivery, *Nat. Mater.* **12**, 991 (2013).
- [12] J. C. Fernández-Toledano, B. Braeckveldt, M. Marengo, and J. De Coninck, How Wettability Controls Nanoprinting, *Phys. Rev. Lett.* **124**, 224503 (2020).
- [13] R. Zhang, S. Farokhirad, T. Lee, and J. Koplik, Multiscale liquid drop impact on wettable and textured surfaces, *Phys. Fluids* **26**, 082003 (2014).
- [14] A. Mahmood, S. Chen, L. Chen, C. Chen, D. Liu, D. Weng, and J. Wang, Spontaneous propulsion of a water nanodroplet induced by a wettability gradient: A molecular dynamics simulation study, *Phys. Chem. Chem. Phys.* **22**, 4805 (2020).
- [15] E. Ni, K. Lu, L. Song, Y. Jiang, and H. Li, Regular self-actuation of liquid metal nanodroplets in radial texture gradient surfaces, *Langmuir* **37**, 13654 (2021).
- [16] X. Wu, J. Di, Z. Yang, and Y. Duan, Molecular dynamics simulation of spreading of mixture droplets on chemically heterogeneous surfaces, *Langmuir* **38**, 8353 (2022).
- [17] J. Koplik and R. Zhang, Nanodrop impact on solid surfaces, *Phys. Fluids* **25**, 022003 (2013).
- [18] K. Kobayashi, K. Konno, H. Yaguchi, H. Fujii, T. Sanada, and M. Watanabe, Early stage of nanodroplet impact on solid wall, *Phys. Fluids* **28**, 032002 (2016).
- [19] T. Koishi, K. Yasuoka, and X. C. Zeng, Molecular dynamics simulation of water nanodroplet bounce back from flat and nanopillared surface, *Langmuir* **33**, 10184 (2017).
- [20] Y. B. Wang, Y. F. Wang, S. R. Gao, Y. R. Yang, X. D. Wang, and M. Chen, Universal model for the maximum spreading factor of impacting nanodroplets: From hydrophilic to hydrophobic surfaces, *Langmuir* **36**, 9306 (2020).
- [21] S. Lv, Z. Yang, and Y. Duan, Retraction kinetics of impacting nanodroplets on hydrophobic surfaces: A molecular dynamics simulation study, *J. Mol. Liq.* **341**, 116936 (2021).

- [22] Q. Ma, Y.-F. Wang, Y.-B. Wang, X. He, S.-F. Zheng, Y.-R. Yang, X.-D. Wang, and D.-J. Lee, Phase diagram for nanodroplet impact on solid surfaces, *Phys. Fluids* **33**, 102007 (2021).
- [23] Y. B. Wang, Y. F. Wang, Y. R. Yang, X. D. Wang, and M. Chen, Spreading time of impacting nanodroplets, *J. Phys. Chem. B* **125**, 5630 (2021).
- [24] Y.-F. Wang, Y.-B. Wang, X. He, B.-X. Zhang, Y.-R. Yang, X.-D. Wang, and D.-J. Lee, Retraction dynamics of low-viscosity nanodroplets: From hydrophobic to hydrophilic surfaces, *J. Mol. Liq.* **355**, 118963 (2022).
- [25] Y.-F. Wang, Y.-B. Wang, X. He, B.-X. Zhang, Y.-R. Yang, X.-D. Wang, and D.-J. Lee, Scaling laws of the maximum spreading factor for impact of nanodroplets on solid surfaces, *J. Fluid Mech.* **937**, A12 (2022).
- [26] S. Gao, Q. Liao, W. Liu, and Z. Liu, Nanodroplets impact on rough surfaces: A simulation and theoretical study, *Langmuir* **34**, 5910 (2018).
- [27] H. Li and K. Zhang, Dynamic behavior of water droplets impacting on the superhydrophobic surface: Both experimental study and molecular dynamics simulation study, *Appl. Surf. Sci.* **498**, 143793 (2019).
- [28] H. Chen, Q. Nie, and H. Fang, Many-body dissipative particle dynamics simulation of Newtonian and non-Newtonian nanodroplets spreading upon flat and textured substrates, *Appl. Surf. Sci.* **519**, 146250 (2020).
- [29] P. Mao, S. Gao, W. Liu, and Z. Liu, Head-on collision of two nanodroplets on a solid surface: A molecular dynamics simulation study, *Langmuir* **37**, 12346 (2021).
- [30] S.-H. Lv, F.-F. Xie, Y.-R. Yang, D.-J. Lee, X.-D. Wang, and Y.-Y. Duan, Impact regimes of nanodroplets impacting nanopillared surfaces, *Phys. Rev. Fluids* **7**, 034203 (2022).
- [31] L. Sun, J. Pan, X. Wang, and D. Jing, Molecular dynamics study of nanoscale droplets impacting on textured substrates of variable wettability, *Phys. Fluids* **34**, 012005 (2022).
- [32] N.-N. Han, B.-M. Sun, and X. He, Oblique impacts of water nanodroplets on superhydrophobic surfaces: A molecular dynamics study, *J. Mol. Liq.* **365**, 120074 (2022).
- [33] H. Zhang, L. Pan, and X. Xie, Molecular dynamics simulation on behaviors of water nanodroplets impinging on moving surfaces, *Nanomaterials* **12**, 247 (2022).
- [34] Y. Noh and N. R. Aluru, Effect of interfacial vibrational coupling on surface wettability and water transport, *Phys. Rev. E* **106**, 025106 (2022).
- [35] R. Li, P. Zhu, Z. Yin, and Y. Xu, Molecular dynamics simulation of nanodroplets impacting stripe-textured surfaces, *Langmuir* **38**, 7058 (2022).
- [36] H. Liu, F. Chu, J. Zhang, and D. Wen, Nanodroplets impact on surfaces decorated with ridges, *Phys. Rev. Fluids* **5**, 074201 (2020).
- [37] N.-N. Han, S.-W. Wang, B.-M. Sun, and X. He, Nanodroplet impacts on hydrophobic/superhydrophobic surfaces with point textures, *J. Appl. Phys.* **132**, 205302 (2022).
- [38] Z. Yin, Z. Ding, X. Ma, X. Zhang, and Y. Xia, Molecular dynamics simulations of single water nanodroplet impinging vertically on curved copper substrate, *Microgravity Sci. Technol.* **31**, 749 (2019).
- [39] M. Zheng, Z. Guo, W. Dong, and X. Guo, Experimental investigation on ice accretion on a rotating aero-engine spinner with hydrophobic coating, *Int. J. Heat Mass Transfer* **136**, 404 (2019).
- [40] S. Feng, J. Delannoy, A. Malod, H. Zheng, D. Quéré, and Z. Wang, Tip-induced flipping of droplets on Janus pillars: From local reconfiguration to global transport, *Sci. Adv.* **6**, eabb4540 (2020).
- [41] X.-H. Li, X.-X. Zhang, and M. Chen, Estimation of viscous dissipation in nanodroplet impact and spreading, *Phys. Fluids* **27**, 052007 (2015).
- [42] B.-X. Li, X.-H. Li, and M. Chen, Spreading and breakup of nanodroplet impinging on surface, *Phys. Fluids* **29**, 012003 (2017).
- [43] Y. R. Zhang and K. H. Luo, Regimes of head-on collisions of equal-sized binary droplets, *Langmuir* **35**, 8896 (2019).
- [44] Y. Xiong, H. Huang, and X. Y. Lu, Numerical study of droplet impact on a flexible substrate, *Phys. Rev. E* **101**, 053107 (2020).
- [45] V. Sanjay, P. Chantelot, and D. Lohse, When does an impacting drop stop bouncing?, *J. Fluid Mech.* **958**, A26 (2023).
- [46] J. Luo, F. Chu, Z. Ni, J. Zhang, and D. Wen, Dynamics of droplet impacting on a cone, *Phys. Fluids* **33**, 112116 (2021).
- [47] A. P. Thompson, H. M. Aktulga, R. Berger, D. S. Bolintineanu, W. M. Brown, P. S. Crozier, P. J. in 't Veld, A. Kohlmeyer, S. G. Moore, T. D. Nguyen *et al.*, LAMMPS—a flexible simulation tool for particle-based materials modeling at the atomic, meso, and continuum scales, *Comput. Phys. Commun.* **271**, 108171 (2022).
- [48] A. Stukowski, Visualization and analysis of atomistic simulation data with OVITO—the open visualization tool, *Model. Simul. Mater. Sci. Eng.* **18**, 015012 (2010).
- [49] J. L. F. Abascal and C. Vega, A general purpose model for the condensed phases of water: TIP4P/2005, *J. Chem. Phys.* **123**, 234505 (2005).
- [50] H. C. Andersen, Rattle: A “velocity” version of the shake algorithm for molecular dynamics calculations, *J. Comput. Phys.* **52**, 24 (1983).
- [51] J. G. Amar, Effects of long-range interactions in metal epitaxial growth, *Phys. Rev. B* **67**, 165425 (2003).
- [52] J. Zhang, M. K. Borg, K. Sefiane, and J. M. Reese, Wetting and evaporation of salt-water nanodroplets: A molecular dynamics investigation, *Phys. Rev. E* **92**, 052403 (2015).
- [53] M. N. Joswiak, N. Duff, M. F. Doherty, and B. Peters, Size-dependent surface free energy and Tolman-corrected droplet nucleation of TIP4P/2005 water, *J. Phys. Chem. Lett.* **4**, 4267 (2013).
- [54] S. Burian, M. Isaiev, K. Termentzidis, V. Sysoev, and L. Bulavin, Size dependence of the surface tension of a free surface of an isotropic fluid, *Phys. Rev. E* **95**, 062801 (2017).
- [55] R. Wang, Y.-Z. Shi, C.-Y. Zhang, and H. Ding, On the maximal spreading of drops impacting onto a no-slip substrate, *Phys. Fluids* **34**, 052103 (2022).
- [56] Y. Zhang, J. E. Sprittles, and D. A. Lockerby, Nanoscale thin-film flows with thermal fluctuations and slip, *Phys. Rev. E* **102**, 053105 (2020).
- [57] C. Zhao, J. E. Sprittles, and D. A. Lockerby, Revisiting the Rayleigh–Plateau instability for the nanoscale, *J. Fluid Mech.* **861**, R3 (2019).
- [58] F. F. Xie, S. H. Lv, Y. R. Yang, and X. D. Wang, Contact time of a bouncing nanodroplet, *J. Phys. Chem. Lett.* **11**, 2818 (2020).

- [59] D. Richard, C. Clanet, and D. Quere, Surface phenomena—contact time of a bouncing drop, *Nature (London)* **417**, 811 (2002).
- [60] X. Cheng, T.-P. Sun, and L. Gordillo, Drop impact dynamics: Impact force and stress distributions, *Annu. Rev. Fluid Mech.* **54**, 57 (2022).
- [61] T. Li, L. Zhang, M. Li, M. Yan, E. Ni, Y. Ruan, and H. Li, Non-retraction rebound of the impacting nano-droplets, *J. Mol. Liq.* **329**, 115521 (2021).
- [62] H.-B. Hu, L.-B. Chen, L.-Y. Bao, and S.-H. Huang, Molecular dynamics simulations of the nano-droplet impact process on hydrophobic surfaces, *Chin. Phys. B* **23**, 074702 (2014).
- [63] B. Zhang, V. Sanjay, S. Shi, Y. Zhao, C. Lv, X.-Q. Feng, and D. Lohse, Impact Forces of Water Drops Falling on Superhydrophobic Surfaces, *Phys. Rev. Lett.* **129**, 104501 (2022).
- [64] J. Li, Macroscopic Model for Head-On Binary Droplet Collisions in a Gaseous Medium, *Phys. Rev. Lett.* **117**, 214502 (2016).
- [65] H.-J. Butt, K. Graf, and M. Kappl, *Physics and Chemistry of Interfaces* (WILEY-VCH Verlag GmbH & Co. KGaA, Weinheim, 2003).
- [66] D. Lohse, Fundamental fluid dynamics challenges in inkjet printing, *Annu. Rev. Fluid Mech.* **54**, 349 (2022).